Biophysical Chemistry, 32 (1988) 173–185
Elsevier

BPC 01320

Lifetime distributions and anisotropy decays of indole fluorescence in cyclohexane / ethanol mixtures by frequency-domain fluorometry

Ignacy Gryczynski [a], Wieslaw Wiczk [a], Michael L. Johnson [b] and Joseph R. Lakowicz [a]

[a] *University of Maryland at Baltimore, School of Medicine, Department of Biological Chemistry, 660 West Redwood Street, Baltimore, MD 21201 and* [b] *University of Virginia, School of Medicine, Department of Pharmacology, Charlottesville, VA 22908, U.S.A.*

Received 25 July 1988
Accepted 29 August 1988

Fluorescence decay; Frequency-domain fluorometry; Lifetime distribution; Indole

We used frequency-domain fluorometry to measure intensity and anisotropy decay of indole fluorescence in cyclohexane/ethanol mixtures at 20 °C. In 100% cyclohexane or 100% ethanol the intensity decay of indole appears to be a single exponential with decay times of 7.66 and 4.10 ns, respectively. In cyclohexane containing a small percentage of ethanol (up to 10%), we observed increased heterogeneity in intensity decay, resulting in a 10-fold increase in χ^2_R for the single-exponential fit, as compared with the double-exponential model. We obtained comparable or better fits using unimodal Lorentzian and Gaussian lifetime distributions (two floating parameters) than for the two-exponential model (three floating parameters). We believe that the distribution of decay times reflects a range of indole solvation states in the dominately nonpolar solutions. This result suggests that a variety of hydrogen-bonding configurations could be one origin of the distributions of decay times observed for tryptophan emission from proteins. We also measured rotational diffusion of indole in cyclohexane, ethanol and its mixtures at 20 °C. The picosecond correlation times required that the mean decay times be decreased by acrylamide quenching (in ethanol) or energy transfer (in cyclohexane). In ethanol we observed nearly isotropic rotation of indole; in cyclohexane we obtained two correlation times of 17 and 73 ps. The shorter correlation time in cyclohexane appears to be due to the slip boundary condition, which was found to be progressively eliminated by small percentages of ethanol. Hence, hydrogen-bonding interactions appear to have a substantial effect on the rotational dynamics of indole.

1. Introduction

Continuous distributions of decay times have recently been used to analyze fluorescence intensity decays [1–8] as an alternative model for a sum of discrete exponential decays [7–12]. A variety of phenomena can result in decay-time distributions, which have been discussed in detail [8]. One interesting case is the fluorescence of single-tryptophan proteins, which is known to be multi- or nonexponential for a number of proteins. One possible origin of this lifetime heterogeneity is a multitude of conformational states [13,14], and it has been experimentally demonstrated that multiple conformations can cause decay time heterogeneity in proteins [15]. The sensitivity of indole and tryptophan fluorescence to the microenvironments has been studied by many authors [16–20] using traditional methods of measurements and of data analysis. The recent development of time-domain [21–23] and frequency-domain [25,26] fluorometers now provides higher statistical accuracy and resolution, even for low degrees of heterogeneity.

To model the heterogeneous environment of proteins we examined indole in cyclohexane/ethanol mixtures. We expected low concentrations of ethanol to result in a variety of partially solvated indole molecules. The data from these samples were analyzed in terms of both multiexponential

Correspondence address: J.R. Lakowicz, University of Maryland at Baltimore, School of Medicine, Department of Biological Chemistry, 660 West Redwood Street, Baltimore, MD 21201, U.S.A.

decays and continuous lifetime distributions. At low concentrations of ethanol we observed interactions between indole and ethanol which alter the indole emission spectra and decay times. These interactions appear to induce a distribution of decay times, which is probably the result of a distribution of indole solvation states.

We also measured the anisotropy decays of indole in the cyclohexane/ethanol mixtures. The fluorescence anisotropy decay depends upon the dynamical properties of the solvent, as well as on the shape, size, interactions with solvent, and optical properties of the rotating molecule [27–31]. Depending upon their spatial symmetry, and slip or stick boundary conditions for interactions with the solvent, molecules can have two or three different rotational diffusion coefficients, resulting in multiexponential anisotropy decays. In low-viscosity solutions (such as ethanol or cyclohexane at room temperature) rotation of small molecules occurs in the range of 100 ps [27]. To obtain adequate data to recover the rotational correlation times it is necessary to decrease the lifetime of the fluorescence. As the lifetime of rotating molecules is decreased, the early time portion of the anisotropy decay contributes increasingly to the data [32–34]. Acrylamide is a generally recommended quencher (collisional quenching) of the indole fluorescence [35,36] and we used it to decrease fluorescence lifetime of indole in ethanol. In nonpolar solvents such as cyclohexane, acrylamide is less soluble and cannot be used as an efficient quencher. We used nonradiative energy transfer [37] to decrease the decay time of indole in cyclohexane. This method requires about 100-fold lower concentration of quencher than collisional quenching and can be used for high- as well as low-viscosity solutions [38].

2. Theory

2.1. Multiexponential decays

Fluorescence intensity decays are usually described as the sum of exponentials

$$I(t) = \sum_i \alpha_i e^{-t/\tau} \tag{1}$$

where τ_i are the individual decay times and α_i the associated preexponential factors. The fractional contribution of the i-th component to the total fluorescence is

$$f_i = \frac{\alpha_i \tau_i}{\sum \alpha_i \tau_i} \tag{2}$$

where $\Sigma f_i = 1$. Since the time- or frequency-domain data are usually collected without regard for the total intensity of the sample, it is also customary to normalize the α_i values so that $\Sigma \alpha_i = 1$.

2.2. Distribution of lifetimes

We consider a model in which the amplitudes α_i are described by a continuous distribution $\alpha(\tau)$. The intensity decay contains components of lifetime τ with an amplitude $\alpha(\tau)$. The component with each τ value is given by

$$I(\tau, t) = \alpha(\tau) e^{-t/\tau} \tag{3}$$

The total decay law is the sum

$$I(t) = \int_{t=0}^{\infty} \alpha(\tau) e^{-t/\tau}\, dt \tag{4}$$

where $\int \alpha(\tau)\, d\tau = 1$. We selected Gaussian (G) and Lorentzian (L) distributions to describe $\alpha(\tau)$. For these functions the $\alpha(\tau)$ values are

$$\alpha_G(\tau) = \frac{1}{\sigma\sqrt{2\pi}} \cdot e^{-\frac{1}{2}\left(\frac{\tau-\bar{\tau}}{\sigma}\right)^2} \tag{5}$$

$$\alpha_L(\tau) = \frac{1}{\pi} \cdot \frac{\Gamma/2}{(\tau-\bar{\tau})^2 + (\Gamma/2)^2} \tag{6}$$

where $\bar{\tau}$ is the central value of the distribution, σ the standard deviation of the Gaussian and Γ the full-width at half-maximum (hw) for the Lorentzian. For a Gaussian the full-width at half-maximum is given by 2.354σ. The use of functional forms for $\alpha(\tau)$ minimizes the number of floating parameters in our fitting algorithms. For these unimodal distributions there are only two floating parameters, hw and $\bar{\tau}$. The more complex multimodal distributions are described elsewhere [8].

In the frequency domain the measured quantities are the phase angle (ϕ_ω) and the demod-

ulation factor (m_ω), where ω refers to the modulation frequency in rad/s. These values can be calculated from the sine (N_ω) and cosine (D_ω) transforms of the impulse response function constructed with assumed parameter values. Using eq. 4 these transforms are

$$N_\omega J = \int_{\tau=0}^{\infty} \frac{\alpha(\tau)\omega\tau^2}{1+\omega^2\tau^2}\,d\tau \tag{7}$$

$$D_\omega J = \int_{\tau=0}^{\infty} \frac{\alpha(\tau)\tau}{1+\omega^2\tau^2}\,d\tau \tag{8}$$

with

$$J = \int_{\tau=0}^{\infty} \alpha(\tau)\tau\,d\tau \tag{9}$$

For any parameter values the calculated (c) phase and modulation values are

$$\phi_{c\omega} = \arctan(N_\omega/D_\omega) \tag{10}$$

$$m_{c\omega} = (N_\omega^2 + D_\omega^2)^{1/2} \tag{11}$$

The parameter values (τ and hw or α_i and τ_i) are selected by comparison of the measured (ϕ_ω, m_ω) and calculated ($\phi_{c\omega}$, $m_{c\omega}$) values by the method of nonlinear least squares [39,40]. The goodness-of-fit was judged by the value of reduced χ_R^2

$$\chi_R^2 = \frac{1}{\nu}\sum_\omega \left(\frac{\phi_\omega - \phi_{c\omega}}{\delta\phi}\right)^2 + \frac{1}{\nu}\sum_\omega \left(\frac{m_\omega - m_{c\omega}}{\delta m}\right)^2 \tag{12}$$

where ν is the number of degrees of freedom, and $\delta\phi = 0.2$ and $\delta m = 0.005$ are the uncertainties in the measured phase and modulation values, respectively.

2.3. Anisotropy decays

The anisotropy decay can be described as a sum of exponentials

$$r(t) = \sum_i r_0 g_i e^{-t/\theta_i} \tag{13}$$

where θ_i are rotational correlation times and $r_0 g_i$ represent the amplitude of the anisotropy which decays via the i-th correlation time. In some of our analyses the individual $r_0 g_i$ values were all variable parameters. This results in the total anisotropy ($r_0 = \Sigma r_0 g_i$) being a variable parameter. In other calculations we constrained the total anisotropy to be equal to the value observed in the absence of rotational diffusion. In this case r_0 is fixed, and the $\Sigma g_i = 1.0$. It should be noted that the correlation times are related, but not equal to, the rotational diffusion coefficients of the fluorophore about its principle axes [28–31].

In the frequency domain, the anisotropy decay is recovered from the difference of the phase angle between the parallel (||) and perpendicular ($\perp$) components of the emission ($\Delta_\omega = \phi_\perp - \phi_\parallel$) and the ratio of the polarized and modulated components of the emission ($\Lambda_\omega = m_\parallel/m_\perp$), each measured over a range of modulation frequencies (ω). For the nonlinear least-squares analysis these values are calculated for an assumed anisotropy decay law using

$$\Delta_{c\omega} = \arctan\left(\frac{D_\parallel N_\perp - N_{\parallel\perp}}{N_\parallel N_\perp + D_\parallel D_\perp}\right) \tag{14}$$

$$\Lambda_{c\omega} = \left(\frac{N_\parallel^2 + D_\parallel^2}{N_\perp^2 + D_\perp^2}\right)^{1/2} \tag{15}$$

where

$$N_i = \int_0^\infty I_i(t)\sin\omega t\,dt \tag{16}$$

$$D_i = \int_0^\infty I_i(t)\cos\omega t\,dt \tag{17}$$

where i represents parallel or perpendicular components of the emission, given by

$$I_\parallel(t) = \tfrac{1}{3}I_0(t)[1 + 2r(t)] \tag{18}$$

$$I_\perp(t) = \tfrac{1}{3}I_0(t)[1 - r(t)] \tag{19}$$

$I_o(t)$ is the decay of the total emission and is given by $I_\parallel(t) + 2I_\perp(t)$. It should be noted that the intensity decay of indole becomes heterogeneous in the presence of a quencher or acceptor due to the nature of quenching (transient effect in quenching of indole [41]) or nonradiative energy transfer. The data were fitted to the multiexponential model (see section 2.1), and the parameters from this analysis (α_i and τ_i) were fixed quantities in eqs. 18 and 19 for the anisotropy analysis.

The goodness-of-fit to the anisotropy decay is also estimated (see eq. 12) from the value of the reduced χ^2_R:

$$\chi^2_R = \frac{1}{\nu}\sum_{\omega}\left(\frac{\Delta_\omega - \Delta_{c\omega}}{\delta\Delta}\right)^2 + \frac{1}{\nu}\sum_{\omega}\left(\frac{\Lambda_\omega - \Lambda_{c\omega}}{\delta\Lambda}\right)^2 \quad (20)$$

where $\delta\Delta = 0.1°$ and $\delta\Lambda = 0.005$ are the uncertainties in the measured values. The modulation data are presented as the modulated anisotropy

$$r_\omega = (\Lambda_\omega - 1)/(\Lambda_\omega + 2) \quad (21)$$

The values of r_ω can be compared with those of the steady-state anisotropy r and the fundamental anisotropy r_0. At low modulation frequencies r_ω is nearly equal to r. At high modulation frequencies r_ω approaches r_0 [42,43].

3. Materials and methods

Frequency-domain measurements were performed using the 2 GHz fluorometer described previously [26]. The laser beam was expanded to about 5 mm in diameter to decrease its local intensity. Indole was excited at 297 nm, and the emission was observed through a WG320 filter, except for solutions containing *trans*-stilbene. In this case we used a 313 nm interference filter with front-face geometry. No fluorescence of *trans*-stilbene was observed at 313 nm. Intensity decays were measured using magic-angle polarization conditions. Indole was purified by HPLC, *trans*-stilbene was of Kodak grade for scintillation, and acrylamide was from Biorad (electrophoresis grade). Solutions not containing *trans*-stilbene or acrylamide were purged by nitrogen to remove dissolved oxygen. All measurements were performed at 20 °C.

4. Results

4.1. Lifetime analysis

Emission spectra of indole in cyclohexane/ethanol mixtures are shown in fig. 1. A small percentage of ethanol results in the loss of structure, increases in the spectral width, and dramatic shifts in the emission to longer wavelengths. This is typical of the fluorescence of polar fluorophores in binary solvents [44]. These spectral changes are most probably due to specific hydrogen-bonding interactions between indole and ethanol, which are enhanced in the nonpolar cyclohexane solvent. It seems probable that the environment surrounding indole is relatively homogeneous in the pure solvents (100% cyclohexane or ethanol). However, a heterogeneous environment might be predicted at low ethanol concentrations due to a statistical distribution of indole molecules which have different numbers of nearby ethanol molecules.

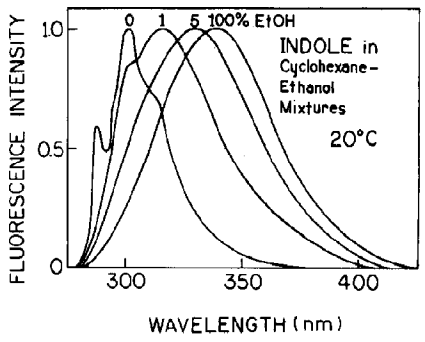

Fig. 1. Emission spectra of indole in cyclohexane, ethanol and mixtures at 20 °C.

We examined the frequency-domain intensity decays of indole using a WG 320 filter, which collects most of the emission above 320 nm. The multiexponential analyses are summarized in table 1. In cyclohexane as well as in ethanol the decays are well approximated by a single-exponential model, giving 7.60 and 4.11 ns respectively, with nearly the same χ^2_R values for the single and the double-exponential fits. Fig. 2 shows the frequency response of the emission of indole in these pure solvents. The lower panels show randomly distributed deviations of the phase and modulation values from the single-exponential model, which further indicates that the decays are singly exponential.

The intensity decays of indole in cyclohexane become heterogeneous in the presence of small amounts of ethanol. This is seen in table 1, which shows the values of χ^2_R for the one- and two-decay-time fits. The highest heterogeneity was ob-

Table 1

Multiexponential analysis of indole intensity decays in cyclohexane/ethanol mixtures at 20 °C

% EtOH	τ_i (ns)	α_i	f_i	χ^2_R
0.0	7.66	1.0	1.0	1.3
	7.49	0.859	0.835	
	8.69	0.146	0.165	1.3
0.5	7.18	1.0	1.0	4.2
	6.09	0.627	0.531	
	9.04	0.373	0.469	0.8
1.0	6.56	1.0	1.0	10.7
	3.84	0.231	0.136	
	7.35	0.769	0.864	1.8
2.5	5.00	1.0	1.0	13.2
	4.40	0.845	0.741	
	8.41	0.155	0.259	2.3
5.0	4.56	1.0	1.0	11.1
	3.86	0.744	0.629	
	6.58	0.256	0.370	1.8
10.0	4.39	1.0	1.0	3.7
	4.24	0.971	0.934	
	9.90	0.029	0.066	1.5
100.0	4.11	1.0	1.0	1.0
	4.04	0.944	0.929	
	5.18	0.056	0.071	1.0

served for mixtures containing 1–5% ethanol, which are also the amounts which produced the largest spectral shifts (fig. 1). In all cases, the data could be fitted using the double-exponential model. This does not prove the decay is doubly exponential, but only that this model is adequate to account for the data.

Since we expect a distribution of indole-ethanol interactions, and since the lifetime of indole is different in cyclohexane and ethanol, it seemed natural to analyze the data in terms of decay time distributions. One such analysis is shown in fig. 3. The data are adequately fitted by a Lorentzian distribution with $\bar{\tau} = 6.46$ ns and hw = 1.36 ns. The value of $\chi^2_R = 1.4$ is equivalent or superior to that found for the double-exponential model ($\chi^2_R = 1.8$, table 1). The data could not be fitted if the half-width was held fixed at a narrow value, 0.01 ns, which becomes equivalent to the single-exponential model. Examination of the lower panels reveals random deviations for the lifetime distribution analysis (hw = 1.36 ns), but systematic deviations if the hw is held constant at 0.01 ns. These results suggest that the intensity decay of indole in cyclohexane with 1% ethanol is indeed described by a distribution of decay times.

Similar evidence for lifetime distributions was found in all the cyclohexane/ethanol mixtures (table 2). In each case we obtained equivalent or superior fits using the distributions as compared with the double-exponential model. It should be noted that only two floating parameters are used in lifetime-distribution analysis ($\bar{\tau}$ and hw), whereas the double-exponential model uses three floating parameters (τ_1, τ_2 and α_1 with $\alpha_1 + \alpha_2 = 1.0$). Comparable fits were obtained using the Lorentzian and Gaussian distributions, so that the present data cannot distinguish between these models. Nonetheless, we have the impression that the Lorentzian model provides slightly superior fits.

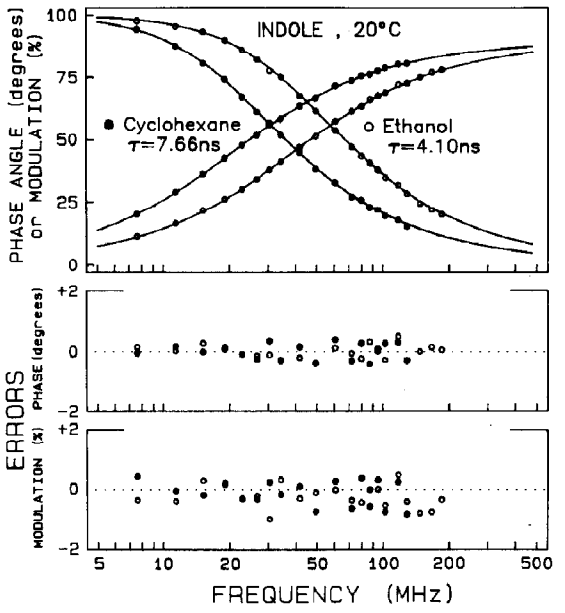

Fig. 2. Frequency response of the emission of indole in cyclohexane (●) and ethanol (○). The solid lines are the best single-decay-time fits to the data.

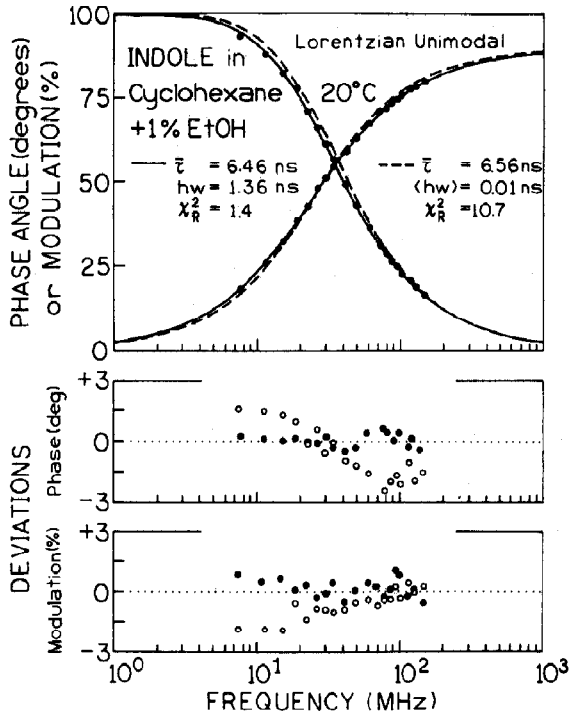

Fig. 3. Phase and modulation data for indole in mixture containing 1% ethanol. Best fits are shown for a one-component Lorentzian (———) with hw = 1.36 ns and with the hw fixed at 0.01 ns (- - - - - -). The lower panel shows the deviation with hw = 1.36 ns (●) and hw = 0.01 ns (○).

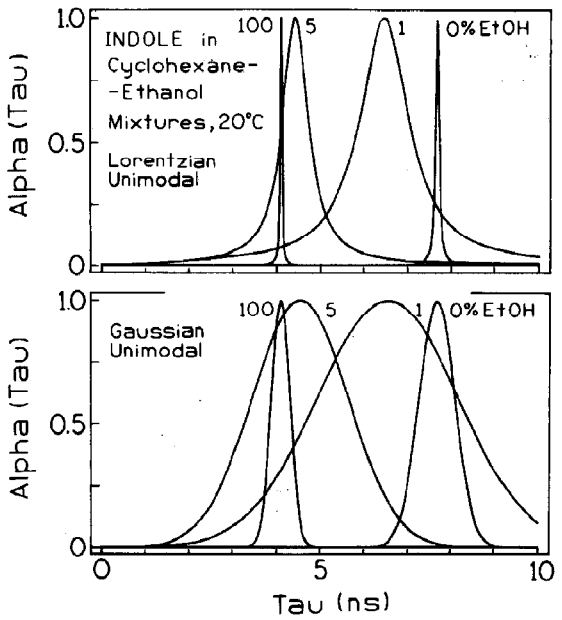

Fig. 4. Distribution of lifetimes recovered for indole in cyclohexane/ethanol mixtures. Top, unimodal Lorentzian; bottom, unimodal Gaussian.

Representative distributions are summarized in fig. 4 for the Lorentzian (top) and Gaussian (bottom) models. The largest half-widths are seen in mixtures containing 1–5% ethanol. Narrow distributions are seen in 100% cyclohexane or ethanol. The decrease in hw seen in 100% ethanol argues against a general effect of ethanol to increase the decay heterogeneity of indole. Comparison of the Lorentzian and Gaussian distributions reveals the latter to be considerably wider. This is because the apparently narrow Lorentzian distributions are the result of the wide tails on this distribution. The data tend to exclude these extreme lifetime values, resulting in apparently narrow lifetime distributions. The Gaussian distributions decay more

Table 2

Lifetime distribution analysis of indole in cyclohexane/ethanol mixtures

[EtOH]	Model					
	Lorentzian			Gaussian		
	$\bar{\tau}$ (ns)	hw (ns)	χ^2_R	$\bar{\tau}$ (ns)	hw (ns)	χ^2_R
0.0	7.68	0.09	1.32	7.66	0.97	1.32
0.5	7.14	0.91	0.89	7.18	3.25	0.80
1.0	6.46	1.36	1.45	6.55	3.81	1.66
2.5	4.86	0.94	1.95	4.98	2.98	2.48
5.0	4.43	0.72	1.85	4.54	2.58	2.00
10.0	4.34	0.32	1.62	4.39	1.69	1.82
100.0	4.10	0.04	1.04	4.10	0.49	1.03

rapidly to zero, so that suppression of the extreme values does not result in the same degree of narrowing. The widths of the Gaussians observed for the single-exponential decays (100% cyclohexane or 100% ethanol) can be regarded as the resolution limits of the measurements, this being a width of 0.5–1.0 ns.

We questioned the uncertainties in the half-widths recovered from the Lorentzian analysis. To accomplish this we examined the values of χ^2_R when the hw was held constant while $\bar{\tau}$ was variable. The least-squares analysis was performed again, allowing the floating parameter to vary, yielding the minimum value of χ^2_R consistent with the fixed half-width. This procedure should account for the correlation between hw and $\bar{\tau}$. These χ^2_R surfaces are shown in fig. 5. The dashed line indicates the value of χ^2_R expected 33% of the time due to random errors. The intersection of the χ^2_R surface with the dashed line approximates the range of half-widths which are consistent with the data, and we believe that this method overestimates their range by about 2-fold. Hence, the χ^2_R surfaces indicate that the data for indole in 100% cyclohexane or ethanol are consistent with a hw of zero, but not with a half-width above 0.2 ns. In contrast, the indole decays in the cyclohexane/ethanol mixtures are not consistent with a hw of zero. The uncertainty in the Lorentzian widths is about 0.2 ns.

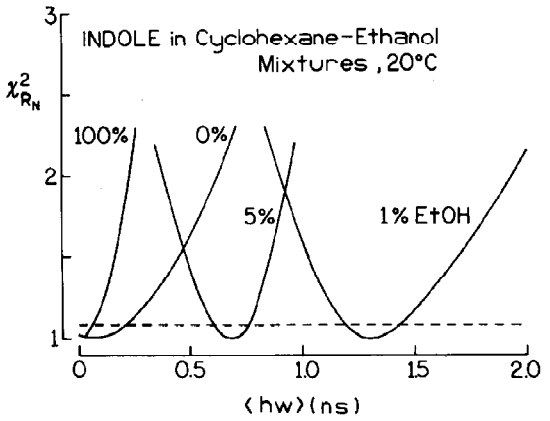

Fig. 5. Dependence of χ^2_R on the full-width of Lorentzian lifetime distributions of indole in cyclohexane/ethanol mixtures. The values were normalized to 1.0 for the minimum value of χ^2_R.

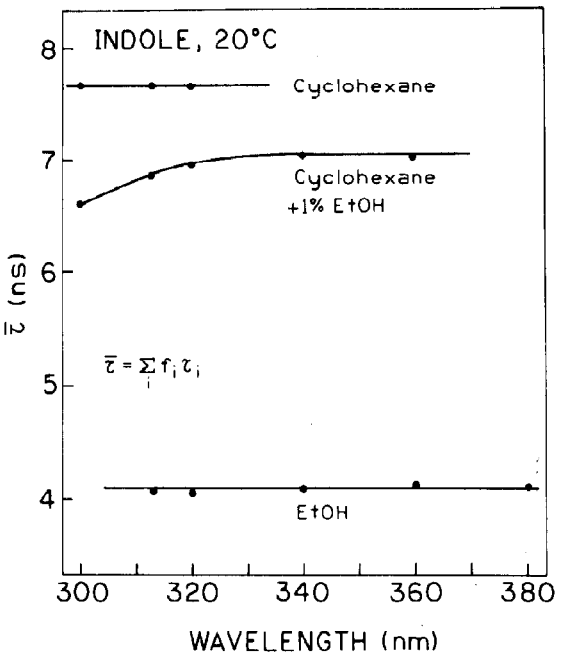

Fig. 6. Emission wavelength dependence of the lifetime of indole in cyclohexane, ethanol and a mixture (1% ethanol).

We questioned whether the complex intensity decays observed in the mixtures were the result of interactions between indole and ethanol present at the moment of absorption (ground-state interactions) or whether the ethanol shell around indole evolved during the lifetime of the excited state (excited-state interactions). One can distinguish between ground-state and excited-state processes by measurements of the intensity decays at various wavelengths across the emission spectrum [45,46]. Hence, we measured the wavelength-dependent intensity decays of indole in 100% cyclohexane, 100% ethanol, and in cyclohexane with 1% ethanol (fig. 6). In cyclohexane, as well as in ethanol, the mean lifetime is constant for each observation wavelength. In the mixture we observed lower mean lifetimes for shorter observation wavelengths. This dependence of lifetime on emission wavelength is characteristic of an excited-state reaction. More specifically, if only ground-state interactions were present then one expects the decay time to decrease at longer wave-

lengths, which select for the shorter-lived emission of indole in ethanol. However, our experiments do not rule out the possibility of a contribution of ground-state heterogeneity to the intensity decays. Rather, the wavelength-dependent increase in decay time suggests that there is at least some dynamic component in the indole-ethanol interactions.

4.2. Anisotropy decays

Previous researchers have suggested that fluorophore-solvent interactions can result in decreased rates of rotational diffusion, or equivalently larger apparent Stokes-Einstein volumes [47]. Hence, we examined the anisotropy decays of indole to determine whether its interactions with ethanol altered the rates of rotational diffusion. For small molecules like indole in low-viscosity solvents, the correlation times are in the range of tens of picoseconds. For example, we measured 52 ps for indole in water at 20 °C [32] and 28 ps in methanol at 5 °C [34]. Because the indole decay times are near 5 ns most of the emission occurs after the anisotropy has decayed to zero, so that the data contain little information about the rates of rotation. This problem can be offset by the use of quenching to decrease the decay time of the molecule. Then, the observed emission is dominately from the early emitting molecules, providing increased information about the early processes [48]. In ethanol, we used acrylamide as a collisional quencher; in cyclohexane and mixtures we used *trans*-stilbene, which quenches the fluorescence of indole by resonance energy transfer. Collisional quenching and/or energy transfer introduce het-

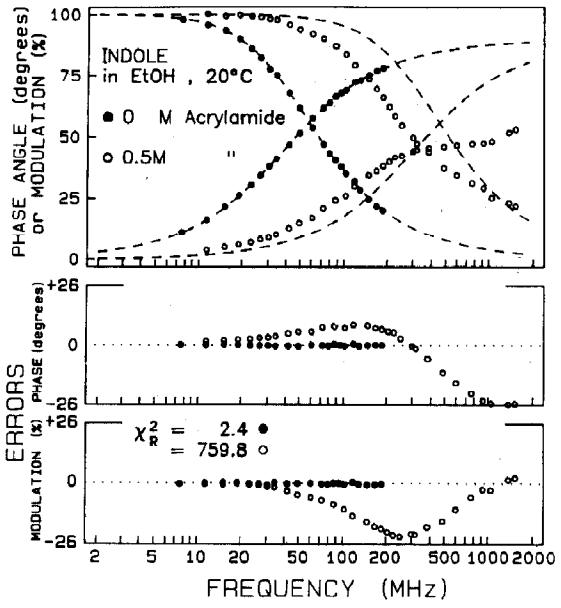

Fig. 7. Frequency response of the emission of indole (in ethanol) with (○) and without 0.5 M acrylamide (●). The dashed lines show the best single-decay-time fit to the data.

Table 3

Multiexponential analysis of quenched indole in cyclohexane/ethanol mixtures at 20 °C

Solvent/quencher	τ_i (ns)	α_i	f_i	χ^2_R
0% EtOH/0.01 M *trans*-stilbene [a]	0.76	1.0	1.0	1768.8
	0.09	0.719	0.159	
	1.25	0.281	0.841	1.9
1% EtOH/0.01 M *trans*-stilbene	0.58	1.0	1.0	1981.9
	0.09	0.754	0.197	
	1.12	0.246	0.803	2.3
5% EtOH/0.01 M *trans*-stilbene	0.54	1.0	1.0	2041.1
	0.08	0.767	0.205	
	1.07	0.233	0.795	2.5
100% EtOH/0.5 M acrylamide	0.20	1.0	1.0	759.8
	0.08	0.847	0.440	
	0.58	0.153	0.560	2.4

[a] For cyclohexane data from ref. 38.

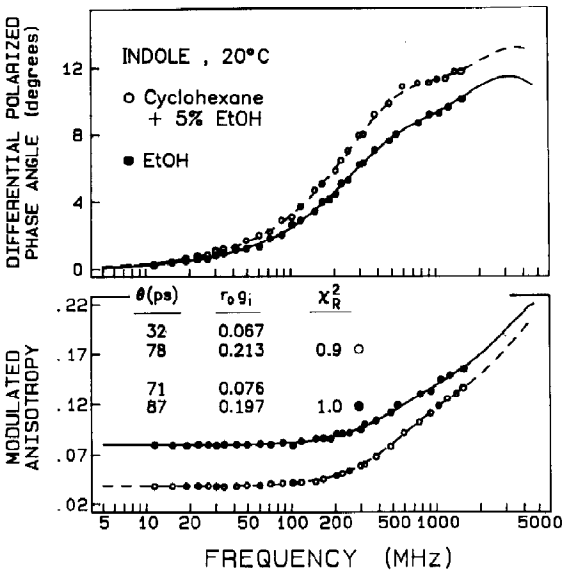

Fig. 8. Frequency-domain anisotropy data for indole in ethanol and a cyclohexane/ethanol mixture (95:5) at 20 °C. The ethanol solution contained 0.5 M acrylamide and the cyclohexane/ethanol (95:5) solution contained 0.01 M *trans*-stilbene.

erogeneity in fluorescence decays. This is illustrated in fig. 7, which shows the indole intensity decays in ethanol, without (●) and with 0.5 M acrylamide (○). In the presence of acrylamide (or *trans*-stilbene) the decay becomes strongly heterogeneous and cannot even be approximated by the single-exponential model ($\chi^2_R = 759.8$). However, this heterogeneity is not a problem because the decays can be parameterized using the double-exponential model (table 3) and these parameters are held fixed during the anisotropy analysis.

The frequency-domain anisotropy data of the quenched indole solutions are shown in fig. 8. Two correlation times were recovered for indole in cyclohexane, 17 and 73 ps (table 4). The same two correlation times were recovered irrespective of whether r_0 was a floating or a fixed parameter. However, the difference in χ^2_R between the one- and two-correlation-time models is considerably larger when r_0 is a fixed value. We attribute the shorter value of 17–22 ps to slip motion of indole (see section 5) and the longer value, 73–75 ps, to rotational diffusion with the stick boundary conditions.

Addition of ethanol appears to eliminate progressively the shorter correlation time. This is seen by an increase from 17 to 31 ps in cyclohexane/

Table 4

Anisotropy decay analysis of indole at 20 °C

Model	$r_0 g_i$	θ_i (ps)	χ^2_R	θ (ps) (stick)	θ (ps) (slip)
Cyclohexane					
r_0-floating					
1θ	0.244	63	1.0	57	19
2θ	0.093	17			
	0.192	73	0.9		
r_0-fixed (0.275 [c])					
1θ	0.275	52	8.9		
2θ	0.095	22			
	0.180	75	0.8		
Cyclohexane/ethanol (99:1)					
r_0-floating					
1θ	0.259	70	0.9		
2θ	0.085	31			
	0.194	82	0.9		
r_0-fixed					
1θ	0.275	64	2.7		
2θ	0.072	32			
	0.203	79	0.8		
Cyclohexane/ethanol (95:5)					
r_0-floating					
1θ	0.266	70	0.8		
2θ	0.082	41			
	0.194	80	0.8		
r_0-fixed					
1θ	0.275	66	1.6		
2θ	0.065	38			
	0.210	78	0.8		
Ethanol					
r_0-floating					
1θ	0.273	83	1.0	68	23
2θ	0.130	81			
	0.142	86	1.0		
r_0-fixed					
1θ	0.275	82	1.0		
	0.103	68			
2θ	0.172	92	1.0		

[a] The values of $\delta\Delta$ and $\delta\Lambda$ in eq. 20 were 0.1° and 0.005, respectively.

[b] Calculated for oblate spheroid and long and short diameters 8.2 and 3.7 Å, respectively. One component (1θ) was calculated as $\theta = (3D_{\|} + 3D_{\perp})^{-1}$; two components ($2\theta$) were calculated as $\theta_1 = (6D_{\perp})^{-1} \approx \theta_3 = 5(D_{\perp} + D_{\|})^{-1}$ and $\theta_2 = (2D_{\perp} + 4D_{\|})^{-1}$ according to Tao [49,50]. Calculations and slip conditions were provided according to Hu and Zwanzig [51].

[c] J.R. Lakowicz and I. Gryczynski, in preparation.

ethanol (99:1) and to 40 ps in cyclohexane/ethanol (95:5), and by a decrease in the amplitude of the short component (table 4). Additionally, the difference in χ^2_R between the one- and two-correlation-time fits is progressively smaller than in pure cyclohexane, indicating that the rotational motions have become more isotropic. The lifetime distribution analysis indicated the probable existence of a number of indole rotational states in this mixture. Hence, it is likely that two correlation times represent a weighted average of these states, and these values should not be assumed to represent any particular indole-ethanol complex. In 100% ethanol the rotation of indole appears to be nearly isotropic, and we found no difference in χ^2_R between the one- and two-correlation-time fits. These results suggest that slip boundary conditions are only found in a nonpolar solvent, and that hydrogen bonding can have a substantial effect in the rotational motions of indole and other polar fluorophores.

We examined the χ^2_R surfaces for the indole correlation times to evaluate the significance of the values listed in table 4. Specifically, we held one correlation time fixed at the value indicated by the x-axis, and again minimized χ^2_R with the other parameters floating. This analysis reveals that the two correlation times observed in cyclohexane are significant and different from each other (———). This distinction is blurred by the addition of 5% ethanol (·–·–·), and is completely eliminated in 100% ethanol (- - - - - -). For indole in ethanol the data are adequate to recover only one correlation time, irrespective of whether r_0 is fixed or variable.

The χ^2_R surfaces also indicate the uncertainties in the correlation times. One estimate of the uncertainty is provided by the least-squares analysis, in particular by the diagonal elements of the covariance matrix [46]. This estimation is correct only if there is no correlation between the fitted parameters. These estimated uncertainties are near 10 and 5 ps for r_0-floating and r_0-fixed models, respectively. A superior estimate is provided by the intersection of the χ^2_R surface with the largest χ^2_R value corrected with random errors in the data. This value of χ^2_R is indicated by the dotted lines in fig. 9. The fact that the χ^2_R surfaces for

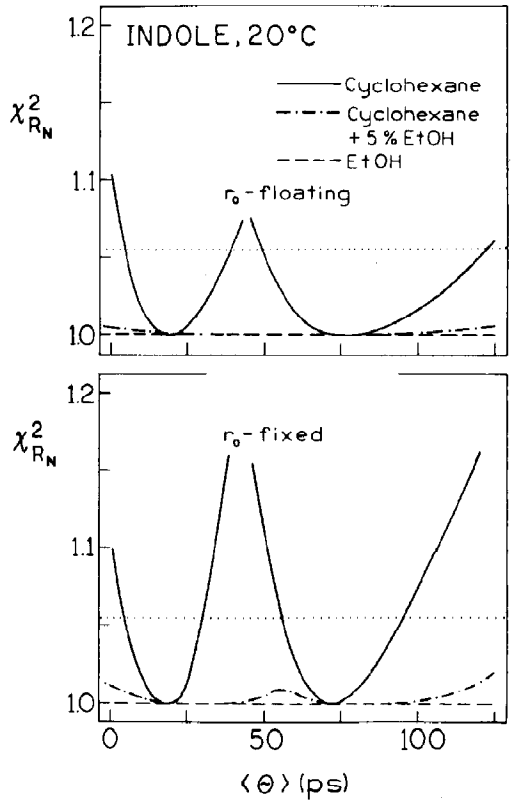

Fig. 9. χ^2_R surfaces for two correlation times of indole in cyclohexane (———), ethanol (- - - - - -) and a mixture containing 5% ethanol (·–·–·). (Top) r_0 was a variable parameter. (Bottom) r_0 was kept constant at the measured value of 0.275.

indole in cyclohexane do not overlap below the line strongly suggests our data are in fact adequate to recover two correlation times, even for these rapid picosecond processes. In contrast, the χ^2_R surfaces for indole in the mixture or in pure ethanol are not strongly dependent on the value of the fixed correlation time from 20 to 70 ps, which suggests that the motions are mostly isotropic.

5. Discussion

The structured and blue-shifted emission spectrum of indole in cyclohexane (fig. 1) shows that interactions between the indole molecules and the surrounding cyclohexane molecules are relatively weak. In contrast, the spectrum is red-shifted and

without structure in ethanol. This effect is due to both specific hydrogen-bonding interactions between the nitrogen from the indole ring and hydroxyl group from ethanol, and the usual dipole-dipole interactions owing to the electric fields created by indole and ethanol.

In mixtures of cyclohexane/ethanol the situation is more complicated. First, there are hydrogen bonds between indole and the trace amounts of ethanol, and these bonds are made stronger due to the low polarity of cyclohexane and the lack of competing species for the hydrogen-bonding interactions. Secondly, the dipole moment of indole changes its value and direction in the excited state. This results in the possible evolution of a new solvent shell during the excited-state lifetime. In contrast to cyclohexane or ethanol, the solvent shell of indole in mixtures is expected to be heterogeneous, just as the C shell is distinct from the Bourne shell. During the lifetime of the excited state, this shell may evolve so as to change both the average number and orientation of the ethanol molecules which surround the fluorophore. We believe that both static and dynamic heterogeneity are the origin of the lifetime distributions observed in mixtures of cyclohexane and ethanol.

It is interesting to note that a similar phenomenon could occur in proteins. More specifically, the indole residues could exist in various hydrogen-bonded configurations, both in the ground state and during the excited-state lifetime. Hence, heterogeneity in hydrogen bonding is one possible origin of the complex decay kinetics which have been observed for proteins.

Since the anisotropy decay is determined by the size and shape of the fluorophore we expect this decay to reflect the interactions of indole with its solvent shell. In fact, this was observed. In cyclohexane, where the interactions are weaker than in ethanol, two correlation times of 17 and 75 ps were recovered. In ethanol these two correlation times collapse into a single value near 80 ps. These results are now considered in terms of slip and stick boundary conditions for rotational diffusion.

The indole molecule can be approximated by an oblate spheroid with diameters 8.2 and 3.7 Å corresponding to longer and shorter axes. The value 3.7 Å corresponds to the thickness of an aromatic ring. The volume of this spheroid is close to that obtained from the density and molecular weight of indole (160 Å^3). The rotational diffusion coefficients of an oblate rotor may be obtained from the solution of the Navier-Stokes equation subject to certain boundary conditions. With the stick boundary condition (Stokes-Einstein Theory)

$$\theta_i = \frac{1}{6D_i} = \eta\lambda_i \frac{v}{kT} = \eta C_i \tag{22}$$

where v is the volume of the molecule, k Boltzmann's constant, T the absolute temperature, and D_i and C_i diffusion and friction coefficients, respectively. The λ_i depend only on the shape of the molecule, and the values are tabulated [49,50]. Hydrodynamics with stick boundary conditions requires that the velocity of the solute molecule surface relative to the nearest solvent molecules is zero. This may occur in systems where strong interactions are present between the fluorophore and the solvent molecules. In systems where the solvent and solute molecules are both of molecular dimensions, and no strong interaction occurs, it is more appropriate to employ slip boundary conditions (i.e., no tangential stress). Here, the resistance to the motion arises from the fact that, for nonspherical molecules, some solvent molecules must be displaced as the fluorophore rotates. The friction coefficient with slip for a spheroid rotating about its symmetry axis is zero. In the slip boundary conditions Pecora and co-workers [52,53] proposed

$$\theta_i = \frac{1}{6D_i} = \eta C_i' + \theta_i^{\circ} \tag{23}$$

with

$$C_i' = \lambda_i' \frac{v}{kT}. \tag{24}$$

The λ_i' have been computed numerically by Hu and Zwanzig [51] for spheroids, and by Youngreen and Acrivos for ellipsoids [54]. The value of θ_i° corresponds to the inertial moment, generally out of reach of fluorescence anisotropy data. For example, for diethyloxadicarbocyanine iodide (DODCI) which is about 2-fold larger than indole, θ_i° was found to be 4 ps [50].

Calculated correlation times for indole are given in table 4. In cyclohexane, the calculated stick boundary correlation time is about 60 ps, and corresponds to a larger correlation time recovered from our data. The slip boundary correlation time of about 19 ps is in good agreement with the shorter correlation time recovered from our anisotropy analysis. In ethanol, the calculated slip boundary correlation time of 23 ps was not found in our experimental data, but the stick boundary correlation time of 70 ps is in agreement with our measurements. In mixtures, where the viscosity is essentially the same as that of 100% cyclohexane, the shorter correlation time increased to 40 ps, suggesting partial elimination of the slip boundary condition. In this case our ability to recover two correlation times is questionable, and the anisotropy decay may already be a single exponential. Hence, our results demonstrate that indole rotation in cyclohexane represents an intermediate situation between stick and slip boundary conditions. Similar intermediate situations have been found for rhodamine 6G and DODCI by Fleming and co-workers [55]. Indole rotation in ethanol represents a clear example of stick boundary condition hydrodynamics. The same condition is dominant in a mixture containing 5% ethanol.

Finally, we note that these observations may be relevant with regard to interpretation of the anisotropy decay of tryptophan (indole) residues in proteins. Depending upon the surrounding structure, the indole group may or may not be hydrogen bonded to the protein. The presence of hydrogen bonding might be expected to eliminate the motions due to slip or oscillatory motions, and thereby eliminate or dampen the amplitudes of the 2–10 ps motions which have been predicted by molecular dynamics simulations [56–58]. In fact, several recent studies of protein dynamics have detected indole correlation times near 70–200 ps for the fast component in the anisotropy decays [33,59,60], which appear to be characteristic of hydrogen-bonded indole.

Acknowledgements

This work was supported by grants DMB-8804931 and DMB-8502835 from the National Science Foundation and GM 39617 from the National Institutes of Health. J.R.L. and W.W. also wish to acknowledge the Medical Biotechnology Center at the University of Maryland.

References

1 D.R. James and W.R. Ware, Chem. Phys. Lett. 120 (1985) 455.
2 D.R. James, Y.S. Liu, P. DeMayo and W.R. Ware, Chem. Phys. Lett. 120 (1985) 460.
3 D.R. James and W.R. Ware, Chem. Phys. Lett. 126 (1986) 7.
4 J.R. Alcala, E. Gratton and F.G. Prendergast, Biophys. J. 51, (1987) 587.
5 J.R. Alcala, E. Gratton and F.G. Prendergast, Biophys. J. 51 (1987) 597.
6 E. Bismuto, E. Gratton and G. Iruce, Biochemistry 27 (1988) 2132.
7 J.R. Alcala, E. Gratton and F.G. Prendergast, Biophys. J. 51 (1987) 925.
8 J.R. Lakowicz, H. Cherek, I. Gryczynski, N. Joshi and M.L. Johnson, Biophys. Chem. 28 (1987) 35.
9 A. Grinvald and I.Z. Steinberg, Anal. Biochem. 59 (1974) 583.
10 J.N. Demas, Excited state lifetime measurements (Academic Press, New York, 1985).
11 D.V. O'Connor and D. Phillips, Time-correlated single photon counting (Academic Press, New York, 1984).
12 J.R. Lakowicz, G. Laczko, H. Cherek, E. Gratton and M. Limkeman, Biophys. J. 46 (1984) 463.
13 R.H. Austin, K.W. Beeson, L. Eisenstein, H. Frauenfelder and I.C. Gansalus, Biochemistry 14 (1975) 5355.
14 A. Ansari, J. Berendzen, S.F. Bowne, H. Frauenfelder, I.E.T. Iben, T.B. Sauke, E. Shyamsunder and R.D. Young, Proc. Natl. Acad. Sci. U.S.A. 82 (1985) 5000.
15 I. Gryczynski, J.R. Lakowicz and M. Eftink, Biochim. Biophys. Acta 954 (1988) 244.
16 A.P. Demchenko, Ultraviolet spectroscopy of proteins (Springer, Berlin, 1986).
17 J.M. Beechem and L. Brand, Annu. Rev. Biochem. 54 (1985) 43.
18 L.F. Gladchenko and L.G. Pikulik, J. Appl. Spectrosc. 6 (1967) 239.
19 M. Sun and P.S. Song, Photochem. Photobiol. 25 (1977) 3.
20 M.S. Walker, T.W. Benar and R. Lumry, J. Chem. Phys. 45 (1966) 3455.
21 A. van Hoek, J. Vervoort and A.J.W.G. Visser, J. Biochem. Biophys. Methods 7 (1983) 243.
22 E.W. Small, L.J. Libertini and I. Isenberg, Rev. Sci. Instrum. 55 (1984) 879.
23 I. Yamazaki and N. Tamai, Rev. Sci. Instrum. 56 (1985) 1187.
24 J.R. Alcala, E. Gratton and D.M. Jameson, Anal. Instrum. 14 (1985) 225.
25 J.R. Lakowicz and B.P. Maliwal, Biophys. Chem. 21 (1985) 61.

26 J.R. Lakowicz, G. Laczko and I. Gryczynski, Rev. Sci. Instrum. 57 (1986) 2499.
27 G.R. Fleming, Chemical applications of ultrafast spectroscopy (Oxford University Press, New York, 1986) ch. 6. (See also J.D. Simon, Acc. Chem. Res. 21 (1988) 128).
28 G.G. Belford, R.L. Belford and G. Weber, Proc. Natl. Acad. Sci. U.S.A. 69 (1972) 1392.
29 E.W. Small and I. Isenberg, Biopolymers 16 (1977) 1307.
30 T.J. Chuang and K.B. Eisenthal, J. Chem. Phys. 57 (1972) 1307.
31 M.D. Barkley, A. Kowalczyk and L. Brand, J. Chem. Phys. 75 (1981) 3581.
32 J.R. Lakowicz, G. Laczko and I. Gryczynski, Biochemistry 26 (1987) 82.
33 J.R. Lakowicz, H. Cherek, I. Gryczynski, N. Joshi and M.L. Johnson, Biophys. J. 51 (1987) 755.
34 J.R. Lakowicz, H. Szmacinski and I. Gryczynski, Photochem. Photobiol. 47 (1988) 31.
35 M.R. Eftink and C.A. Ghiron, J. Phys. Chem. 80 (1976) 486.
36 M.R. Eftink and C.A. Ghiron, Anal. Biochem. 114 (1981) 199.
37 T. Förster, Ann. Phys. (Leipzig) 2 (1948) 55.
38 J.R. Lakowicz, I. Gryczynski and W. Wiczk, Chem. Phys. Lett. 149 (1988) 134.
39 J.R. Lakowicz, E. Gratton, G. Laczko, H. Cherek and M. Limkemann, Biophys. J. 46 (1984) 463.
40 E. Gratton, J.R. Lakowicz, B. Maliwal, H. Cherek, G. Laczko and M. Limkemann, Biophys. J. 46 (1984) 479.
41 J.R. Lakowicz, J.L., Johnson, I. Gryczynski, N. Joshi and G. Laczko, J. Phys. Chem. 91 (1987) 3277.
42 B.P. Maliwal and J.R. Lakowicz, Biochim. Biophys, Acta 873 (1986) 161.
43 B.P. Maliwal, A. Hermetter and J.R. Lakowicz, Biochim. Biophys. Acta 873 (1986) 173.
44 J.R. Lakowicz, Principles of fluorescence spectroscopy (Plenum, New York, 1983).
45 J.R. Lakowicz and A. Balter, Biophys. Chem. 16 (1982) 99.
46 J.R. Lakowicz and A. Balter, Biophys. Chem. 16 (1982) 117.
47 W.W. Mantulin and G. Weber, J. Chem. Phys. 66 (1977) 4092.
48 G. Weber and J.R. Lakowicz, Chem. Phys. Lett. 22 (1973) 419.
49 T. Tao, Biopolymers 8 (1969) 609.
50 G.R. Fleming, Chemical applications of ultrafast spectroscopy (Oxford University Press, New York, 1986) ch. 6.
51 C.M. Hu and R. Zwanzig, J. Chem. Phys. 60 (1974) 4354.
52 G.R. Alms, D.R. Bauer, J.I. Brauman and R. Pecora, J. Chem. Phys. 59 (1973) 5321.
53 D.R. Bauer, G.R. Alms, J.I. Brauman and R. Pecora, J. Chem. Phys. 61 (1979) 2255.
54 G.K. Youngreen and A. Acrivos, J. Chem. Phys. 63 (1975) 3846.
55 G.R. Fleming, A.E.W. Knight, J.M. Morris, R.J. Robins and G.W. Robinson, Chem. Phys. Lett. 51 (1977) 399.
56 M. Karplus and J.A. McCammon, CRC Crit. Rev. Biochemistry 9 (1981) 293.
57 R.M. Levy and A. Szabo, J. Amer. Chem. Soc. 104 (1982) 2073.
58 T. Ichize and M. Karplus, Biochemistry 22 (1983) 2884.
59 T.M. Nordlund, X.Y. Liu and J.H. Sommer, Proc. Natl. Acad. Sci. U.S.A. 83 (1986) 8977.
60 J.W. Petrick, J.W. Longworth and G.R. Fleming, Biochemistry 26 (1987) 2711.